Abnormal bundling and accumulation of F-actin mediates tau-induced neuronal degeneration *in vivo*

Tudor A. Fulga[1,3], Ilan Elson-Schwab[1], Vikram Khurana[1], Michelle L. Steinhilb[1], Tara L. Spires[2], Bradley T. Hyman[2] and Mel B. Feany[1,3]

Hyperphosphorylated forms of the microtubule-associated protein (MAP) tau accumulate in Alzheimer's disease and related tauopathies and are thought to have an important role in neurodegeneration. However, the mechanisms through which phosphorylated tau induces neurodegeneration have remained elusive. Here, we show that tau-induced neurodegeneration is associated with accumulation of filamentous actin (F-actin) and the formation of actin-rich rods in *Drosophila* and mouse models of tauopathy. Importantly, modulating F-actin levels genetically leads to dramatic modification of tau-induced neurodegeneration. The ability of tau to interact with F-actin *in vivo* and *in vitro* provides a molecular mechanism for the observed phenotypes. Finally, we show that the Alzheimer's disease-linked human β-amyloid protein (Aβ) synergistically enhances the ability of wild-type tau to promote alterations in the actin cytoskeleton and neurodegeneration. These findings raise the possibility that a direct interaction between tau and actin may be a critical mediator of tau-induced neurotoxicity in Alzheimer's disease and related disorders.

Members of the MAP family bind and stabilize microtubules in a manner that is regulated by phosphorylation of the MAPs at serine and threonine residues[1,2]. In addition, increasing evidence suggests that tau and other MAPs can interact directly or indirectly with the actin cytoskeleton[3–8]. However, *in vitro* experiments using purified proteins that examined the ability of tau to interact with actin have yielded conflicting results, raising concerns regarding the *in vivo* relevance of this interaction[9–13]. Intriguingly, actin-rich paracrystalline inclusions (known as Hirano bodies) have been described in Alzheimer's disease and other tauopathies, including Pick's disease[14–17], but despite their discovery over 30 years ago, their mechanism of formation and role in neurodegenerative diseases remain poorly understood. On the basis of these findings and studies in yeast, and mammalian cell culture models directly implicating actin stabilization and aggregation in activating cell death[18–21], we hypothesized that a direct interaction between abnormally hyperphosphorylated tau and the actin cytoskeletal network mediates neuronal degeneration in Alzheimer's disease and related disorders. We tested this hypothesis in *Drosophila,* which has recently been established as a useful model system for studying human tauopathies[22–25], as well as in a mouse model of tauopathy.

In *Drosophila*, wild-type human tau exhibits toxicity, as do mutant forms of tau found in familial fronto-temporal dementia linked to chromosome 17 (FTDP–17) including the R406W, V337M and P301L mutants. The mutant forms of tau often show enhanced toxicity[22,23,26]. Similarly, although wild-type human tau can show substantial toxicity

when expressed in transgenic mice[27,28], many mouse models use transgenic expression of FTDP–17-associated mutant human tau. Mutant forms of tau, such as P301L, which is expressed in the rTg4510 transgenic strain used in this study[29,30], produce striking neurotoxicity, even when expressed in the presence of endogenous mouse tau.

RESULTS

Tau interacts with and stabilizes actin filaments *in vitro* and *in vivo*

To determine whether changes in the actin cytoskeleton accompany neurodegeneration, we first investigated the effects of panneural expression in *Drosophila* of R406W mutant tau (tau^R406W) using the *elav–GAL4* driver. Immunofluorescence microscopy analysis of whole-mount brains revealed a substantial increase in the total levels of filamentous (F)-actin in transgenic flies compared with control (*elav–GAL4/+*) flies as detected by rhodamine–phalloidin staining (Fig. 1a). To determine whether this effect was due to a change in the monomeric (G)-actin to F-actin ratio as a consequence of F-actin accumulation, total filamentous actin was precipitated from fresh brain extracts using biotinylated phalloidin and actin levels were determined by immunoblotting. Compared with controls (*elav–GAL4/+*), tau^R406W-expressing flies showed a marked increase in the total F-actin levels, whereas G-actin levels remained unaffected (Fig. 1b). F-actin was then isolated from whole-brain extracts of transgenic flies and the precipitated material was probed for tau.

[1]Department of Pathology, Brigham and Women's Hospital and Harvard Medical School, Harvard New Research Building Room 652, 77 Louis Pasteur Avenue, Boston, MA 02115, USA. [2]Department of Neurology, Massachusetts General Hospital, Charlestown, MA 02129, USA.
[3]Correspondence should be addressed to T.A.F. and M.B.F. (e-mail: Tudor_Fulga@hms.harvard.edu; mel_feany@hms.harvard.edu)
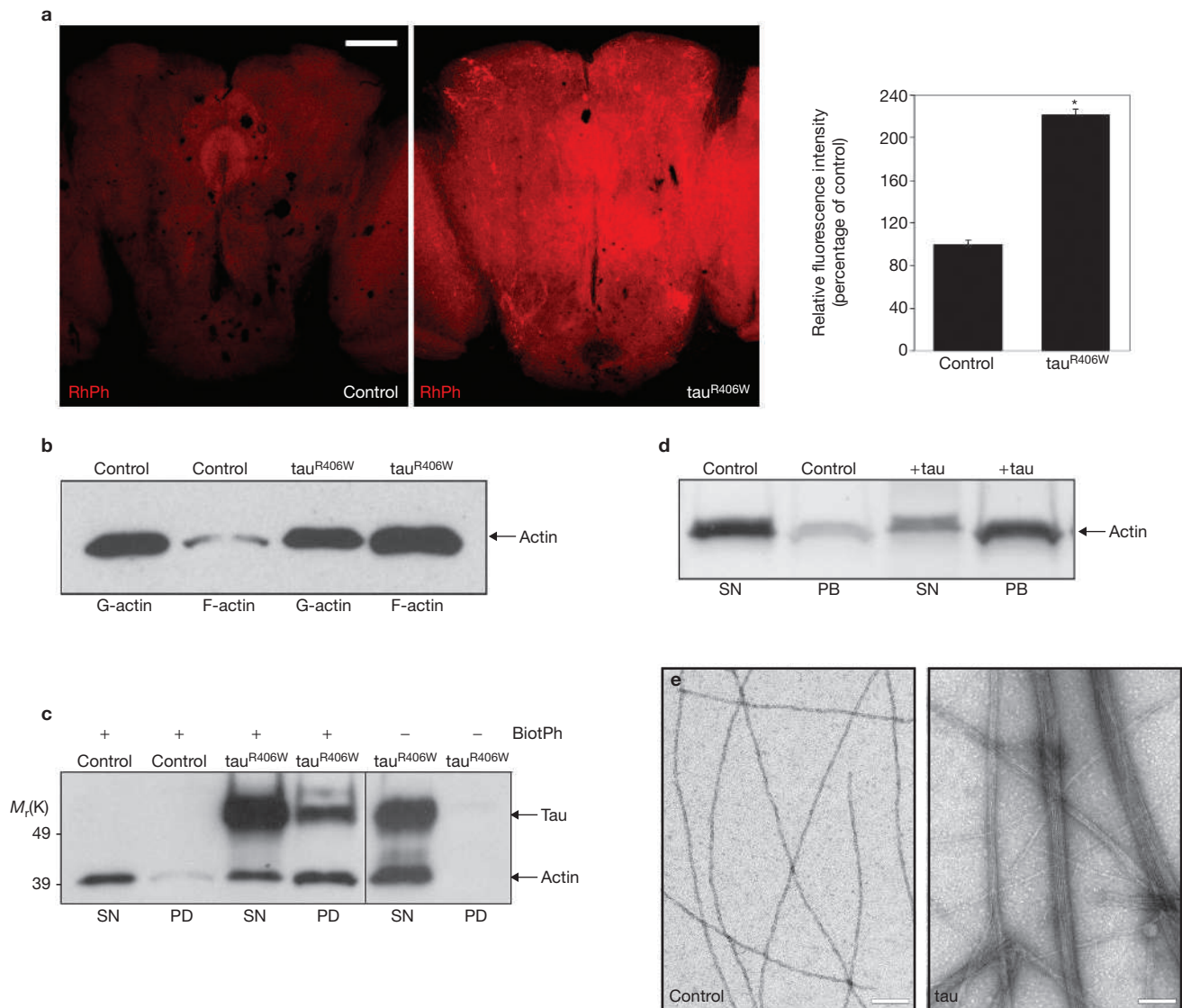
Figure 1 Interaction between tau and the actin cytoskeleton induces abnormal F-actin bundling and accumulation. (a) Rhodamine–phalloidin (RhPh) staining of whole-mount brains from control flies (elav–GAL4/+) compared with tau[R406W] transgenic flies. Images represent the central body of the fly brain. Quantitative analysis of fluorescence intensities averaged from three distinct areas of the brain are also shown. Statistically significant differences from control groups are indicated (unpaired t-test; asterisk indicates $P < 0.0001$) and the error bars represent ± s.e.m. ($n = 3$). (b) Total G-actin and phalloidin-bound F-actin levels isolated from fresh brain extracts of control and tau[R406W] flies and assessed by western blot using an antibody against actin. (c) Coprecipitation of phalloidin-bound F-actin and human tau[R406W] from transgenic fly brains. BiotPh, biotin–phalloidin. (d) Incubation of actin filaments with tau followed by low speed centrifugation results in formation of bundled actin filaments detected in the pellet fraction (PB), whereas individual filaments remain in the supernatant (SN). Samples were separated on SDS–PAGE and detected by Coomassie Blue staining. (e) Negatively stained electron micrographs of pre-sedimentation material shows striking tau-induced F-actin parallel bundles. The scale bars represent 20 μm in a and 100 nm in e.

Western blotting revealed that a significant fraction of tau protein coprecipitated with F-actin (Fig. 1c), indicating that tau can interact with filamentous actin in vivo in Drosophila neurons.

To examine the possibility that tau increased F-actin levels through a crosslinking mechanism, in vitro polymerized actin filaments were incubated with or without purified bovine tau. A low-speed sedimentation assay was then used to quantitatively asses the ability of tau to induce F-actin bundling. In the absence of tau, F-actin was mainly found in the soluble fraction and only a small amount was found in the pellet (bundled F-actin). However, in the presence of tau there was a marked increase of bundled F-actin in the pellet fraction and a concomitant decrease in soluble individual actin filaments (Fig. 1d). To confirm that the

actin-filament bundling activity was due to tau, rather than a contaminant, tau was immunodepleted from the original protein preparation, and the experiment repeated. No bundling was observed in the tau-immunodepleted sample confirming the specific ability of tau to bundle actin filaments (see Supplementary Information, Fig. S1a). Pre-incubation of in vitro polymerized F-actin with tau resulted in increased filament resistance to treatment with Swinholide-A, an F-actin depolymerizing drug, suggesting that tau-induced actin bundling results in stabilization of actin filaments (see Supplementary Information, Fig. S1b). Electron microscopic analysis of presedimentation material revealed that, in the absence of tau, F-actin was predominantly organized as separate individual actin filaments. In contrast, pre-incubation of actin filaments with
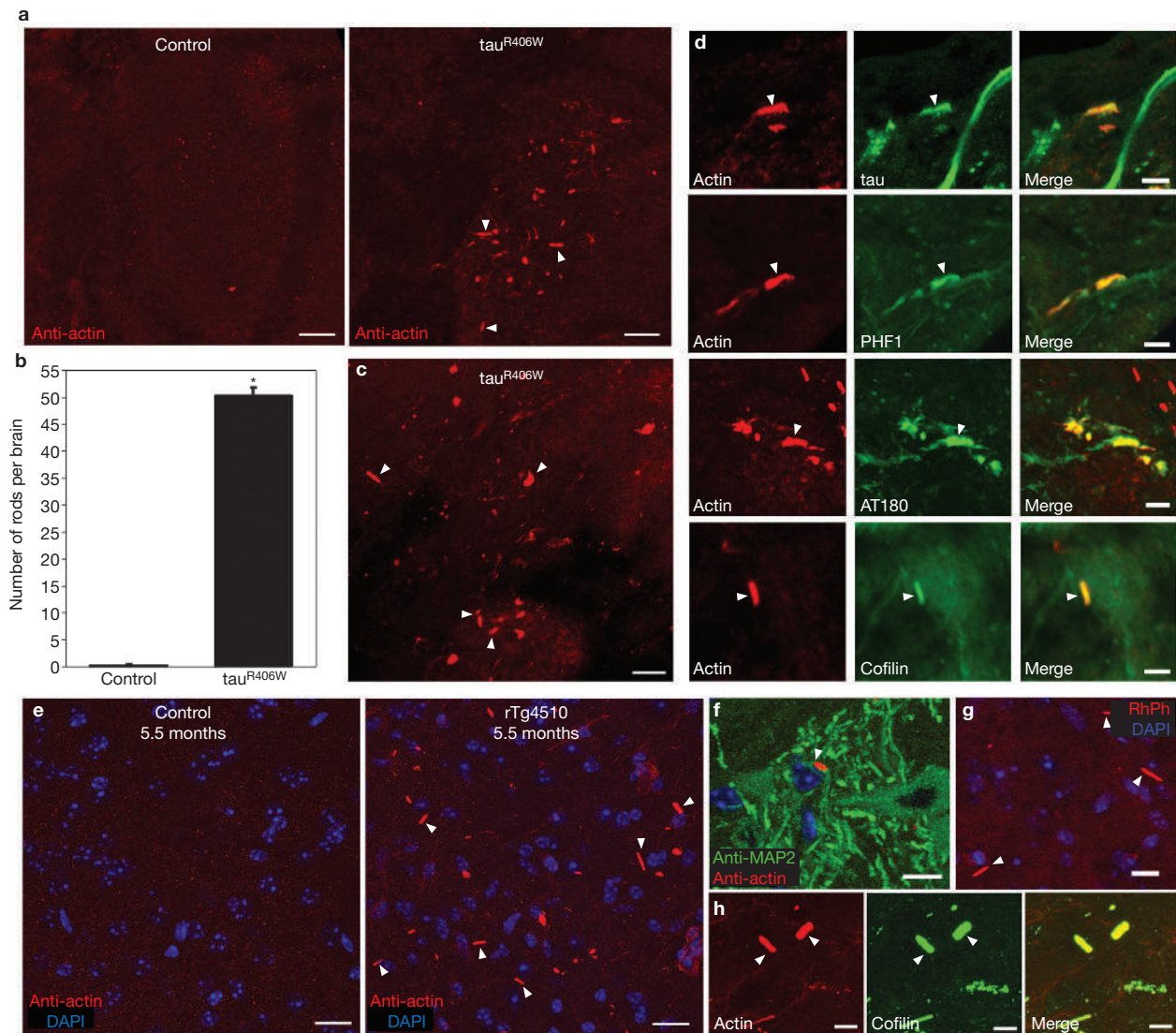
Figure 2 Actin-rich rod formation accompanies neurodegeneration in the brains of tau transgenic flies and mice. (**a**) Immunofluorescence microscopy of frontal brain sections reveals actin-rich rod-like structures (rods) in tau[R406W] transgenic flies (arrowhead). (**b**) Quantification of actin-rich rods in transgenic flies compared with control flies. Statistically significant differences from control groups are indicated (unpaired *t*-test; asterisk indicates *P* <0.0001) and the error bars represent ± s.e.m. (*n* = 6). (**c**) Rods identified by rhodamine–phalloidin staining of whole-mount brains from tau[R406W] transgenic flies. (**d**) Colocalization of actin in rods with *Drosophila* cofilin, human tau, PHF1 and AT180. (**e**) Immunofluorescence staining using an actin antibody shows numerous actin rich-rods in brains of 5.5-month-old tau transgenic mice (rTg4510; arrowheads). (**f**) Costaining of mouse brains with actin and MAP2 antibodies shows the presence of actin rods within neuronal cell bodies. (**g**) Rods stain with rhodamine–phalloidin in coronal brain sections from tau transgenic mice (arrowheads). (**h**) Actin rods also contain cofilin as observed by colocalization of actin and mammalian cofilin. The scale bars represent 10 μm in **a**, **c** and **f**–**h**, 5 μm in **d** and 20 μm in **e**.

tau resulted in the formation of closely packed parallel bundles (Fig. 1e). These results are consistent with previous *in vitro* studies[11] and indicate that tau induces actin-filament bundling *in vitro* and F-actin accumulation *in vivo*, most likely through a direct interaction with F-actin.

Hirano body-like structures form in *Drosophila* and mouse models of tauopathies

We next explored whether structures analogous to Hirano bodies were formed in transgenic flies expressing tau[R406W]. Confocal microscopic analysis of frontal brain sections immunostained for actin revealed the presence of numerous rod-shaped structures throughout the fly brain (Fig. 2a, b and Supplementary Information, Fig. S2a, b). Rod-like inclusions were also highlighted by rhodamine–phalloidin in whole-mount fly brains (Fig. 2c) and double staining with an actin antibody and rhodamine–phalloidin revealed that the majority of rod-shaped structures recognized by the actin antibody contained filamentous actin (see Supplementary Information, Fig. S2c). A substantial proportion of actin-rich rods also contained cofilin and tau, including tau phosphorylated at sites recognized by PHF-1 and AT-180, two disease-associated phosphoepitope-specific monoclonal antibodies (Fig. 2d). Tau immunoreactivity and the ability to bind both actin depolymerizing factor (ADF), cofilin and phalloidin, which are normally mutually exclusive actin-binding agents[31], are features of Hirano bodies from human tissue[16,32,33], supporting an analogy between the actin-rich structures observed in *tau* transgenic flies and authentic Hirano bodies formed in Alzheimer's disease.
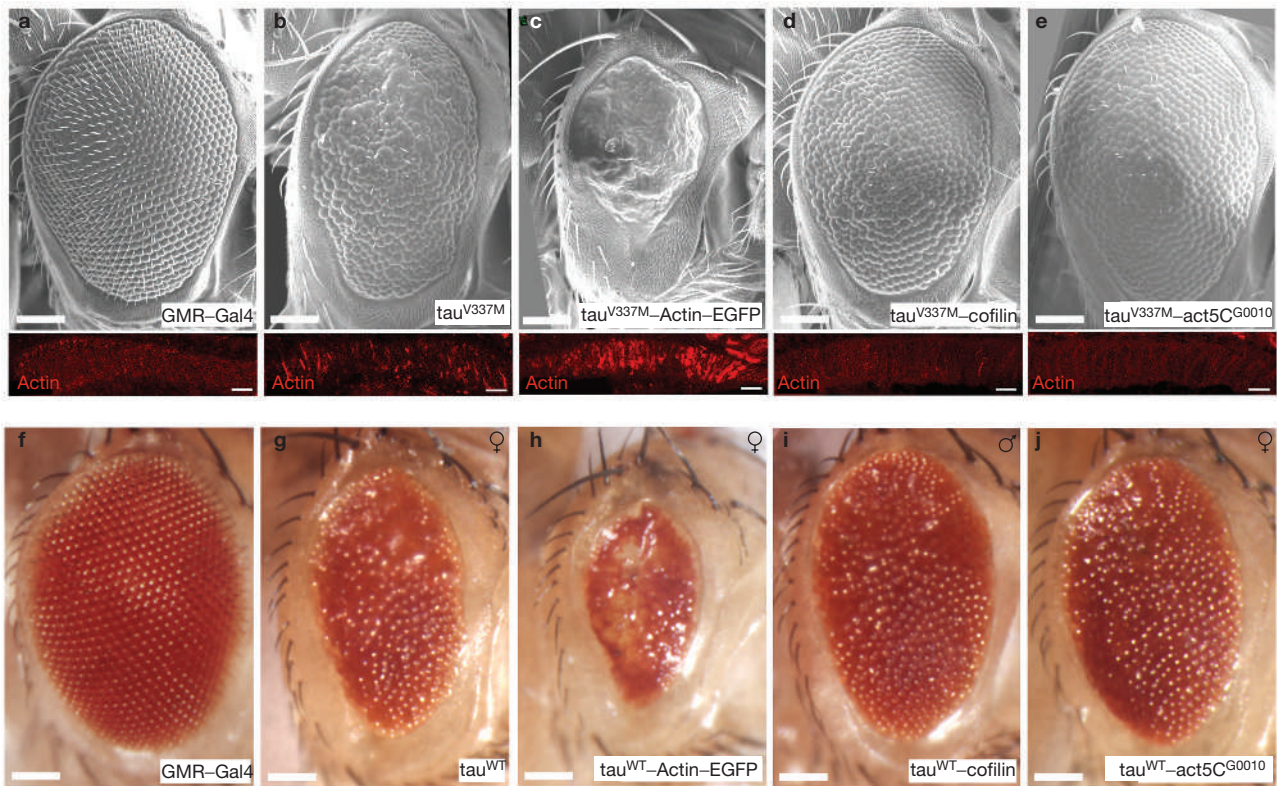
Figure 3 Changes in F-actin modulate neurotoxicity in the retina of tau transgenic flies. (**a**–**e**) Genetic modulation of filamentous actin levels alters tau^{V337M}-induced retinal toxicity. Scanning electron microscopy analysis reveals a rough eye phenotype in tau^{V337M} transgenic flies (**b**) compared with control eyes (*GMR–GAL4/+*; **a**). Tau^{V337M}-induced retinal toxicity is enhanced in transgenic flies coexpressing tau^{V337M} and a *UAS-actin5C-EGFP* transgene (**c**) and strongly suppressed in flies coexpressing tau^{V337M} and a *UAS–cofilin* transgene (**d**), or tau^{V337M} in a genetic background heterozygous for a null actin allele (*Act5C^{G0010}*; **e**). The lower panels (red) indicate actin immunofluorescence staining of a crosssection through photoreceptor projections in the lamina of the flies shown in **a**–**e**. (**f**–**j**) Genetic modulation of F-actin has similar effects on wild-type tau-induced retinal toxicity. Compare normal eye structure (**f**) with single transgenic wild-type tau-induced rough eye (**g**) and flies coexpressing wild-type tau and a *UAS–actin5C–EGFP* transgene (**h**), wild-type tau and a *UAS–cofilin* transgene (**i**) or wild-type tau in a genetic background heterozygous for a null actin allele (*Act5C^{G0010}*; **j**). Male and female flies are indicated. The scale bars represent 100 µm except in the lower panels of **a**–**e** where they represent 10 µm.

To determine whether actin changes accompany neurodegeneration in a vertebrate model of tauopathy, we analysed a transgenic mouse strain (rTg4510) that expresses the tau^{P301L}–FTDP-17-associated mutant form of tau. Previous studies revealed progressive memory impairment, accumulation of hyperphosphorylated tau and region specific neuronal loss in these mice[29,30,34]. Immunofluorescence microscopy analysis of parasaggital brain sections from rTg4510 *tau* transgenic mice revealed the formation of prominent actin-rich rods in areas that contained marked PHF-1 immunoreactivity, including areas that undergo pronounced neurodegeneration such as the cortex, as well as areas such as the striatum that, despite accumulating phosphorylated tau, seem to undergo little neuronal loss (Fig. 2e). Actin rods were present within neuronal cell bodies, as indicated by MAP2 staining (Fig. 2f), as well as in neuronal processes. No colocalization was observed with glial fibrillary acidic protein (GFAP), indicating that rods were not formed in astrocytes (data not shown). Similarly to Hirano bodies and the actin-rich rods formed in *tau* transgenic flies, the rods observed in mice were rich in F-actin as indicated by rhodamine–phalloidin staining (Fig. 2g) and were immunoreactive for cofilin (Fig. 2h). These results strongly support our model in which specific alterations of the actin cytoskeleton accompany tau-induced pathology.

Genetic manipulation of the actin cytoskeleton alters tau-induced neuronal toxicity

In *Drosophila*, targeted retinal expression of tau, including wild-type tau and two forms of mutant tau (tau^{R406W} and tau^{V337M}), results in retinal toxicity observed in adults at eclosion as a rough eye[22,23,35,36] (Fig. 3a, b). For genetic analysis, we selected a line of tau^{V337M}-expressing flies[35] that has a moderate rough eye and is a good substrate for genetic modification. Coexpressing an actin transgene (*UAS–Act5C–EGFP*;*GMR–GAL4* driver) markedly enhanced tau^{V337M}-induced toxicity (Fig. 3c). Overexpression of the *actin* transgene alone increased actin levels, as determined by western blotting or by immunofluorescence microscopy analysis of retinal neurons in tissue sections, but had only a minor effect on eye morphology (see Supplementary Information, Fig. S2d, e, h and i). Additionally, coexpressing tau^{V337M} with an EGFP transgene (*UAS–EGFP*) had no effect on tau-induced retinal toxicity, indicating an actin specific effect of the *UAS–Act5C–EGFP* transgene (see Supplementary Information, Fig. S2f, g). Coexpressing cofilin–Twinstar (*UAS–tsr*), a protein known to sever and destabilize actin filaments, significantly suppressed the rough eye (Fig. 3d). A heterozygous actin null allele (*Act5C^{G0010}*), which decreased total actin levels (see Supplementary Information, Fig. S2k, l), also dominantly suppressed the tau-induced retinal toxicity (Fig. 3e). Of the two *Drosophila* cytoplasmic actin
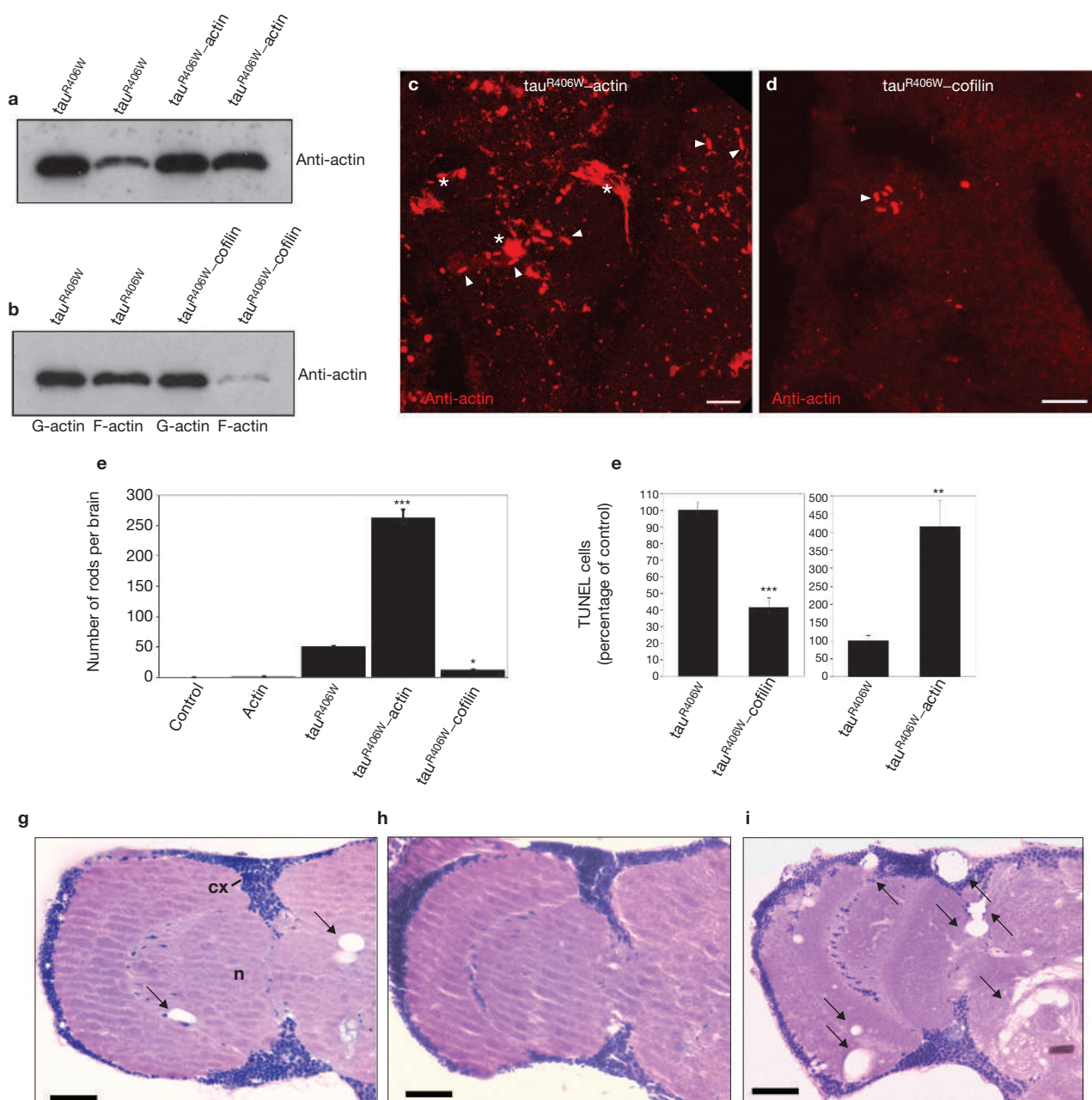
Figure 4 F-actin accumulation and actin-rich rod formation correlate with the degree of tau-induced neuronal degeneration. (**a–b**) Total G-actin and F-actin levels isolated from fresh brain extracts of flies expressing tau^{R406W} compared with flies co-expressing tau^{R406W} with actin (**a**; flies grown at 21 °C) or tau^{R406W} with cofilin (**b**; flies grown at 25 °C). (**c–d**) Immunofluorescence microscopy analysis of rods in frontal brain sections from flies coexpressing tau^{R406W} with actin (**c**) or with cofilin (**d**). Arrowheads indicate individual rods and asterisks indicate areas with dense accumulations of rods and other actin-rich structures. (**e**) Quantification of actin-rich rods in transgenic fly brains expressing tau^{R406W} alone or in an actin-modified genetic background (one-way ANOVA with Student-Neuman-Keuls; single asterisk indicates $P<0.05$; three asterisks indicate $P<0.001$; error bars represent ± s.e.m., $n \geq 4$). (**f**) Quantification of TUNEL-positive neurons in tau^{R406W}-expressing flies compared with flies coexpressing tau^{R406W} with cofilin or tau^{R406W} with actin (unpaired t-test, double asterisk indicates $P<0.01$; three asterisks indicate $P<0.001$; error bars are ± s.e.m., $n = 4$). (**g–i**) Hematoxylin and eosin-stained frontal-brain sections from flies expressing tau^{R406W} (**g**), coexpressing tau^{R406W} with cofilin (**h**) or tau^{R406W} with actin (**i**). Vacuolization of the neuropil (n) and cortex (cx) is indicated by arrows. The scale bars represent 10 μm in **c** and **d**, and 20 μm in **g–i**.

isoforms, Act5C was manipulated in these studies because the *act5C* locus is essential and the *act5C* transcript is enriched in the fly nervous system[37]. Genetic manipulation of the actin cytoskeleton altered the toxicity of wild-type tau in a similar fashion to that of tau^{V337M}, indicating that the observed phenotypes are not only restricted to the mutant forms of human tau (Fig. 3f–j). Abnormal actin accumulation in

photoreceptor projections in the lamina of tau^{V337M} transgenic flies indicated that retinal toxicity was also accompanied by changes in the actin cytoskeleton (Fig. 3b). An excellent correlation was observed between the severity of the rough-eye phenotype and the accumulation of actin in the photoreceptor projections in the lamina in actin-modified genetic backgrounds (Fig. 3c–e).
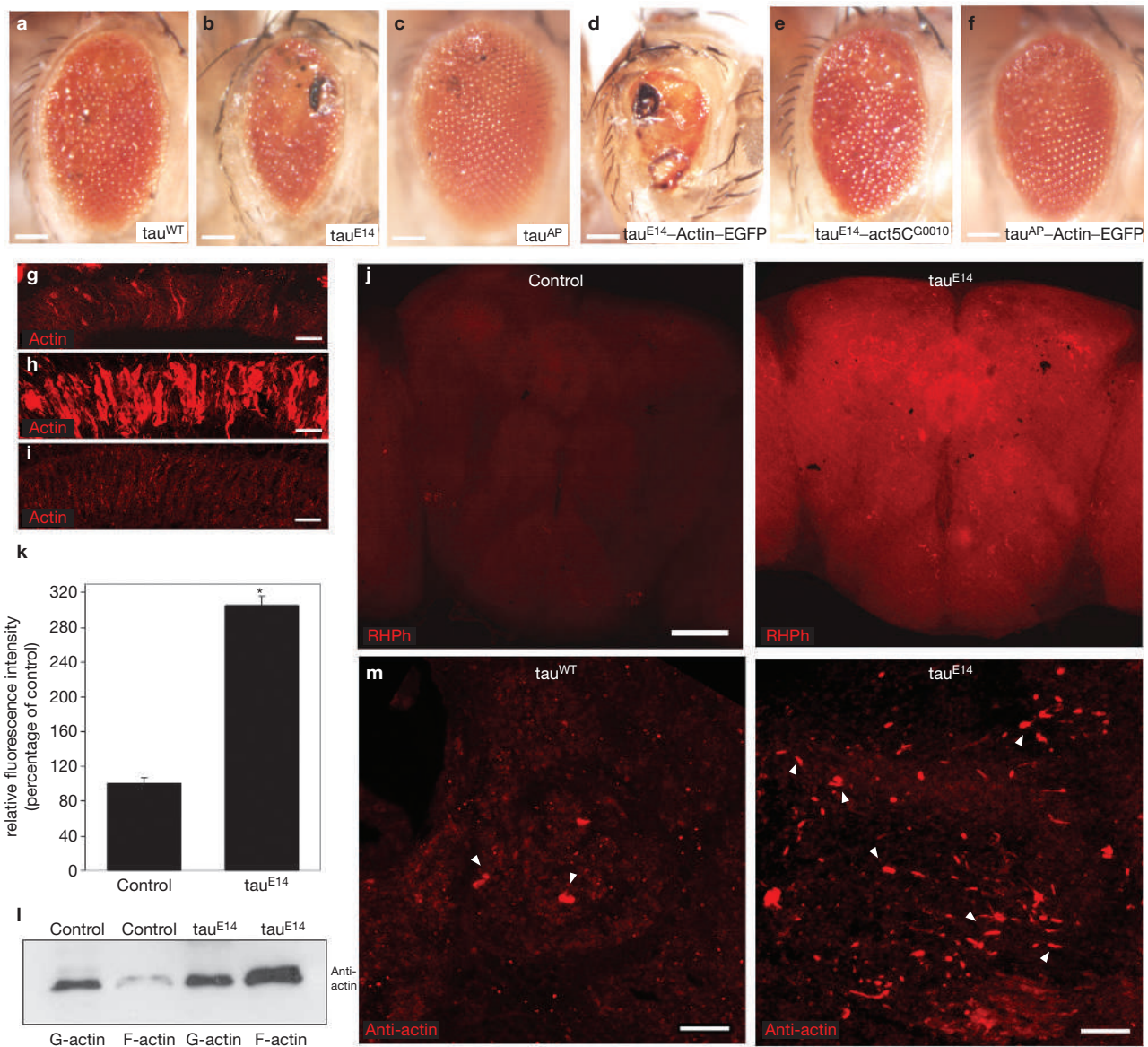
Figure 5 Changes in the actin cytoskeleton occur downstream of tau phosphorylation. (**a–f**) Retinal toxicity in transgenic flies expressing human wild-type tau (**a**), the pseudophosphorylated tau^{E14} mutant (**b**), the phosphorylation-dead tau^{AP} mutant (**c**), tau^{E14} with an actin transgene (**d**), tau^{E14} in a genetic background heterozygous for a null actin allele (**e**) or tau^{AP} with an actin transgene (**f**). (**g–i**) Corresponding immunofluorescence staining of photoreceptor projections in the lamina from transgenic flies expressing wild-type tau (**g**), tau^{E14} (**h**) and tau^{AP} (**i**). (**j–k**) Rhodamine–phalloidin staining of whole-mount brains (**j**) and quantification of fluorescence intensity (unpaired t-test; single asterisk indicates $P < 0.0001$; error bars represent ± s. e.m., $n = 3$; **k**) of control flies and tau^{E14} transgenic flies. (**l**) Total G-actin and F-actin levels isolated from fresh brain extracts of control flies and tau^{E14} transgenic flies. (**m**) Frontal brain sections indicating the abundance of rods in flies expressing the pseudophosphorylated tau^{E14} construct compared with flies expressing wild-type tau. Arrowheads point to individual rods. The scale bars represent 100 μm in **a–f**, 10 μm in **g–i** and **m**, and 20 μm in **j**.

Changes in actin cytoskeleton correlate with the degree of tau-induced neuronal degeneration

To determine whether a relationship exists between neurotoxicity, F-actin levels and actin-rich rod formation, tau was pan-neurally expressed in genetically modified actin backgrounds. Flies coexpressing tau and actin showed a marked increase in total F-actin compared with tau expresison alone, without any significant increase in the levels of G-actin (Fig. 4a). Conversely, pan-neural coexpression of cofilin with tau decreased brain F-actin levels to those of non-transgenic control flies (Fig. 4b). Although expressing actin alone did not induce rod formation (driver *elav–GAL4*; Fig. 4e), coexpression of actin and tau^{R406W} strikingly increased the number of rods throughout the brain neuropil (Fig. 4c, e). These rods efficiently incorporated transgenically expressed actin as indicated by colabelling for actin and GFP (see Supplementary Information, Fig. S2j). Conversely, flies coexpressing tau and cofilin showed a marked reduction in the number of actin-rich rods (Fig. 4d, e). These changes correlated well with neurodegeneration in the brain, as assessed by quantifying TUNEL-positive neurons and by counting the number of degenerative vacuoles — methods previously used to quantify neurodegeneration in *Drosophila*[22,25,36]. The number of TUNEL-positive neurons was dramatically enhanced in flies coexpressing actin and tau compared with flies expressing tau alone (Fig. 4f), whereas flies coexpressing cofilin showed

a greater than 50% reduction in the number of TUNEL-positive cells (Fig. 4f). Similarly, vacuole numbers were decreased by coexpressing tau with cofilin and substantially enhanced by coexpressing tau with actin, compared with tau alone (Fig. 4g–i; Supplementary Information, Fig. S3f). Expressing actin alone in the brain did not result in neuronal toxicity, as assessed by morphology and TUNEL quantification (data not shown). Together, these results strongly suggest that tau-induced bundling and accumulation of F-actin has an important role in mediating neurodegeneration in this model system.

To further validate the correlation between the degree of tau-mediated toxicity and the alterations of the actin cytoskeleton, we also analysed the effect of pan-neural expression of wild-type tau. We have previously shown that, at equivalent levels, transgenic expression of tau[R406W] induces substantially more toxicity than wild-type tau in our *Drosophila* tauopathy model[22]. Accordingly, no detectable actin changes were observed in flies expressing wild-type tau at equivalent levels to tau[R406W] (see Supplementary Information, Fig. S3a–d). The observed alterations in the actin cytoskeleton thus correlate well with the degree of tau toxicity. Flies expressing much higher levels of wild-type tau exhibited significant neurodegeneration and changes in the actin cytoskeleton qualitatively similar to tau[R406W]-expressing flies (data not shown and see Supplementary Information, Fig. S3e).

Actin changes occur downstream of tau phosphorylation

We next explored the relationship between genetic modification of the actin cytoskeleton and tau phosphorylation, which is considered an important pathogenic event in Alzheimer's disease and related tauopathies[2,22,23,25,35]. Western blot analysis of two tau disease-associated phosphoepitopes, AT-8 and PHF-1, in actin-modified genetic backgrounds revealed no significant changes in either of these epitopes despite dramatic modification of toxicity (see Supplementary Information, Fig. S3g), suggesting that changes in the actin cytoskeleton may occur downstream of tau phosphorylation. To further address this issue, two mutant forms of tau were used in which 14 disease-associated Ser–Thr–Pro phosphorylation sites have been mutated either to alanine (tau[AP]) or to glutamate (tau[E14]). The phosphorylation-incompetent tau[AP] construct shows significantly reduced toxicity (M.L.S. and M.B.F., unpublished observations), whereas the pseudophosphorylated tau[E14] is substantially more toxic than wild-type tau[36]. Retinal expression of tau[E14] (driver, *GMR–GAL4*) produced substantial toxicity (Fig. 5b) and induced striking accumulations of actin in the photoreceptor projections in the lamina (Fig. 5h) compared with wild-type tau (Fig. 5a, g). Conversely, overexpression of tau[AP] induced a mild rough-eye phenotype (Fig. 5c; M.L.S. and M.B.F., unpublished observations) and no detectable actin accumulation in the lamina (Fig. 5i). In contrast with wild-type tau (see Supplementary Information, Fig. S3), pan-neural expression (driver, *elav–GAL4*) of tau[E14] at equivalent levels induced a substantial increase in the brain F-actin levels, as revealed by rhodamine–phalloidin staining and by comparing the G- to F-actin ratio in total brain homogenates (Fig. 5j–l). Accordingly, a marked accumulation of actin-rich rods throughout the brain of these flies was observed (Fig. 5m). Although tau[E14]-induced retinal toxicity was clearly modified by genetically modulating the actin cytoskeleton (Fig. 5d, e), the tau[AP]-induced rough eye was not enhanced by coexpressing actin (Fig. 5f). Taken together, these results support a model in which tau phosphorylation is required to induce changes in the actin cytoskeleton that mediate tau-induced neurodegeneration.
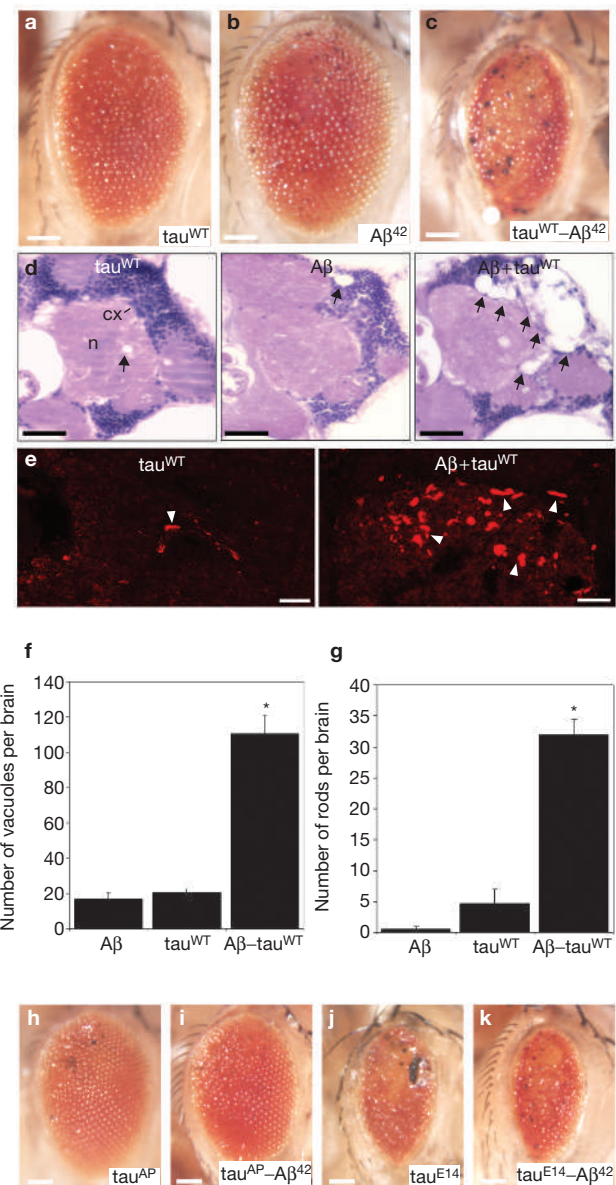

Figure 6 Aβ and tau interact in a synergistic manner to promote actin-rich rod formation and neuronal degeneration. (**a**–**c**) Retinal toxicity in flies expressing wild-type tau (**a**), Aβ (**b**) and double-transgenic flies expressing wild-type tau and Aβ (**c**). (**d**) Hematoxylin and eosin-stained frontal brain sections from flies expressing wild-type tau, Aβ or coexpressing wild-type tau and Aβ indicates that Aβ substantially enhances wild-type tau-induced neurodegeneration. Vacuolization of the neuropil (n) and cortex (cx) is indicated by arrows. (**e**) Flies expressing wild-type tau alone have only occasional actin-rich rods (arrowhead), whereas Aβ-tau double-transgenic flies show a striking increase in the number and frequency of rods (arrowheads). (**f**–**g**) Quantification of the number of vacuoles (**f**) and actin rods (**g**) throughout the brain of these flies supports a synergistic interaction between wild-type tau and Aβ (one-way ANOVA with Student-Neuman-Keuls; single asterisk indicates $P < 0.001$;). Error bars represent ± s. e.m. ($n \geq 3$). (**h**–**k**) Enhancement of tau toxicity by Aβ is mediated in part by changes in tau phosphorylation. Retinal toxicity in flies expressing mutant tau[AP] (**h**), double-transgenic flies coexpressing tau[AP] and Aβ (**i**), flies expressing mutant tau[E14] (**j**) and flies coexpressing tau[E14] and Aβ (**k**). No changes in the tau[E14] or tau[AP]-induced retinal toxicity were observed in the double-transgenic flies coexpressing Aβ. The scale bars represent 100 μm in **a**–**c** and **h**–**k**, 20 μm in **d** and 10 μm in **e**.

Aβ potentiates the ability of tau to induce changes in the actin cytoskeleton and neuronal death

As noted above, Hirano bodies have been observed in Alzheimer's disease, as well as in other tauopathies. In Alzheimer's disease, Aβ accumulation is thought to be upstream of tau phosphorylation and neuronal toxicity[38]. Studies in mice showed that Aβ increases tau hyperphosphorylation and tangle formation, suggesting a functional interaction between Aβ and tau[39,40]. We investigated whether Aβ can genetically interact with wild-type tau in our model and whether changes in the actin cytoskeleton may underlie this interaction. To establish an Alzheimer's disease-relevant model of this interaction in *Drosophila*, double-transgenic flies were engineering that coexpressed an *Aβ* transgene[41] and wild-type *tau*. Although retinal expression of either wild-type tau or Aβ alone resulted in a mild rough eye (Fig. 6a, b), coexpression of both transgenes strongly enhanced retinal toxicity (Fig. 6c), indicating a synergistic interaction between tau and Aβ. Analysis of the adult brain revealed a substantial increase in the number of vacuoles (Fig. 6d, f) as well as in the number of TUNEL-positive cells (see Supplementary Information, Fig. S4) in the brains of aged double-transgenic flies, compared with either transgene alone (Fig. 6d, f and see Supplementary Information, Fig. S4), further indicating a synergistic interaction between tau and Aβ.

Aβ may enhance tau-induced neurodegeneration by potentiating the ability of tau to stabilize the actin cytoskeleton. To examine this hypothesis, frontal brain sections from double-transgenic flies expressing Aβ and wild-type tau were immunostained for actin. Although flies expressing Aβ alone showed no detectable actin changes, and only occasional actin-rich rods were observed in wild-type tau transgenic flies, double-transgenic flies showed a striking increase in the number of actin-rich rods, suggesting that the synergistic interaction between Aβ and tau may be mediated by alterations in the actin cytoskeleton (Fig. 6e, g). To further explore the relationship between Aβ and tau toxicities in our system, tau and tau–Aβ-induced retinal toxicities were examined in an actin-modified genetic background. The generation of these flies required a genetic background different to the flies shown in Fig. 6a and c, and the slight enhancement in retinal toxicity observed in the tau transgenic flies and double-transgenic flies coexpressing tau and Aβ is attributable to this difference. Interestingly, the heterozygous *Act5C*[G0010] allele produced a substantial rescue of both the tau and tau–Aβ induced toxicities, despite the significant initial enhancement of tau toxicity by Aβ (see Supplementary Information, Fig. S4b–e). These findings support the hypothesis that the synergistic enhancement of tau by Aβ was mediated, at least in part, by tau-induced actin cytoskeletal changes.

To determine whether tau phosphorylation is required for the synergistic interaction between tau and Aβ, the ability of Aβ to enhance retinal toxicity of tau[AP] and tau[E14] mutants was assessed. Although the coexpression of wild-type tau with Aβ resulted in enhanced retinal toxicity (Fig. 6a–c), double-transgenic flies coexpressing Aβ and either tau[AP] or tau[E14] showed no clear change in retinal toxicity (Fig. 6h–k). Thus, the interaction between Aβ and tau seems to require intact Ser/Thr phosphorylation sites on tau.

Actin cytoskeletal changes are specific to tau-induced neuronal toxicity

To determine whether alterations in the actin cytoskeleton are a common mechanism mediating neurodegeneration, we analysed whether actin changes also accompanied or modulated a distinct form of neurodegeneration in flies. Machado Joseph Disease (MJD) is a neurodegenerative disorder caused by abnormal polyglutamine expansion of the ataxin 3 protein. In *Drosophila,* expression of polyglutamine-expanded ataxin 3 leads to apoptotic neurodegeneration in the fly brain[42] and a rough-eye phenotype in the retina[43]. Interestingly, no genetic (see Supplementary Information, Fig. S3h, i) or immunohistochemical (data not shown) evidence was found for a role for abnormal F-actin accumulation in the fly model of MJD. These data are consistent with a tau-specific role for actin cytoskeletal changes in neurodegeneration and correlate with the specific interaction of tau with F-actin that we demonstrate.

DISCUSSION

Although mutant tau causes neurodegeneration in familial fronto-temporal dementias, and the extent of tau pathology correlates well with neuronal loss in Alzheimer's disease and related tauopathies[2], the direct downstream targets of tau that mediate neurodegeneration have not been delineated. Identification of actin as a tau-interacting protein *in vivo* and an important downstream effector of tau-induced degeneration raises the possibility that actin cytoskeletal changes are not epiphenomenal events, but are important mediators of toxicity in tauopathies. As Aβ and tau synergistically interact to stabilize actin and induce neurodegeneration, our results may have particular relevance for Alzheimer's disease. A correlation between F-actin accumulation and the formation of actin-rich rods in the fly brain suggests that tau-dependent F-actin accumulation may directly lead to rod formation, and potentially to analogous structures (such as Hirano bodies) noted in human disease. However, it remains unclear whether the rods themselves mediate toxicity or represent a neuronal protective mechanism in response to abnormal F-actin accumulation.

Further investigation will be required to define the events downstream of tau-induced F-actin bundling and accumulation that mediate neuronal degeneration. Interestingly, recent studies in other systems have directly implicated F-actin stabilization and aggregation in activating apoptotic cell death. In yeast, manipulations that decrease actin turnover and induce accumulation of aggregated F-actin, triggered an elevation in reactive oxygen species (ROS) levels, apoptosis and decreased lifespan[18]. Experiments in cultured cortical neurons showed that reorganization of the actin cytoskeleton by the actin depolymerizing protein gelsolin could protect cultured neurons from apoptosis (by enhancing actin dynamics and thus preventing the loss of mitochondrial membrane potential and the activation of pro-apoptotic caspase-3; refs 44). Furthermore, accumulation of oxidative-damage markers as a consequence of increased ROS levels has been observed in brain tissue from Alzheimer's disease patients[45], and oxidative stress is a key mediator of tau toxicity in our *Drosophila* model[49]. It will be interesting to determine whether a direct correlation exists between tau-induced F-actin accumulation, oxidative stress and neuronal cell death in tauopathies.

Crosstalk between the actin microfilament network and the microtubule cytoskeleton is thought to underlie many basic cellular processes during development and adult life[46]. Our results suggest that when components of these cytoskeletal networks become abnormally regulated, this crosstalk can have dramatic consequences for neurons, potentially leading to the nerve-cell death observed in Alzheimer's disease and related disorders. □

METHODS

Fly stocks and transgenes. All flies were age and sex-matched when assessing modification of brain and eye toxicity. Fly crosses and experiments were performed at 25 °C unless noted otherwise. The human *UAS–tau*, *UAS–tau[R406W]* and *UAS–tau[V337M]* transgenic lines were previously described[22]. The *UAS–tau[E14]* transgenic line was generated by mutating fourteen disease-associated Ser–Thr–Pro phosphorylation sites (Thr 111, Thr 153, Ser 175, Thr 181, Ser 199, Ser 202, Thr 205, Thr 212, Thr 217, Thr 231, Ser 235, Ser 396, Ser 404 and Ser 422) to glutamate[36], whereas the *UAS–tau[AP]* transgenic line was generated by mutating the same sites to alanine (M.L.S. and M.B.F, unpublished observations). Lines with expression level equivalent to wild-type tau were previously determined by quantitative western blot analysis. The pan-neural driver used was *elav–GAL4* and the retinal driver was *GMR–GAL4,* both obtained from Bloomington *Drosophila* Stock Center (Bloomington, IN). The *act5C[G0010]* mutant line was also obtained from Bloomington and the *UAS–Actin5C–EGFP* transgene was a generous gift from P. Rörth (European Molecular Biology Laboratory, Heidelberg, Germany). The cofilin–Twinstar transgenic flies (*tsr*) were generated by injecting fly embryos with a *p(UAS)His-tsr* plasmid which was a generous gift from T. Uemura (Kyoto University, Kyoto, Japan). The UAS–Aβ42 transgene was a kind gift from D. Garza (Novarits Institutes of Biomedical Research, Cambridge, MA).

Immunocytochemistry and histology. The primary antibodies used were anti-actin (1:200, A-2066; Sigma, St Louis, MO), Tau1 (1:1,000; Chemicon, Temecula, CA), PHF-1 (1:200; a generous gift from P. Davies, Albert Einstein College of Medicine, Bronx, NY), AT180 (1:500; Innogenetics, Ghent, Belgium), anti-cofilin (1:200; Cytoskeleton, Denver, CO), anti-MAP2 (1:200; Sigma-Aldrich, St Louis, MO), and anti-Dcofilin–Twinstar (1:200; a generous gift from T. Uemura[47]). For immunohistochemistry in *Drosophila*, adult flies were fixed in formalin and embedded in paraffin. Serial-frontal sections (4 μm), including the entire brain, were prepared. Mouse brains were fixed in formalin and either embedded in paraffin or cryoprotected in glycerol. Parasaggital sections (16 μm) of paraffin-embedded material were prepared. Antigen retrieval was performed by microwaving in sodium citrate buffer. Immunostaining was performed using secondary antibodies coupled to Alexa-Fluor 488 or Alexa-Fluor 555. Vibratome sections (50 μm) were stained with rhodamine–phalloidin. Samples were analysed on a Zeiss laser-scanning confocal microscope.

To assess brain morphology, sections were stained using hematoxylin and eosin using a standard protocol. The degree of degeneration was determined by counting vacuoles larger than 3 μm in well-oriented frontal sections, including the entire brain, from 10-day-old flies grown either at 25 °C or at 21 °C, as specified in the figure legends. At least four individual hemibrains were analysed per genotype.

Confocal microscopy. To determine the total F-actin staining in adult fly brains, whole brains from 1-day-old flies were dissected as previously described[48] and stained with rhodamine–phalloidin (Molecular Probes, Inc., Carlsbad, CA). Before acquisition, laser parameters were adjusted to obtain nonsaturating conditions. Samples were processed simultaneously using identical confocal acquisition parameters (laserpower, gain and pinhole settings) on a BioRad Radience laser-scanning confocal microscope. For quantification of fluorescent staining, average pixel intensity from two-dimensional projections of confocal *z*-stacks acquired in three independent regions of the brain, including approximately 50% of the total brain, were measured using the MetaMorph image analysis software (Universal Imaging, Downingtown, PA).

The number of actin-rich rods was determined by counting all rod-shaped and round structures over 3 μm in size that positively stained for actin in 4 μm frontal brain sections including the entire brain, from flies grown and aged as specified above. At least four hemibrains were analysed per genotype.

F-actin isolation, coprecipitation studies and immunoblotting. To isolate total F-actin, brains from 1-day-old flies were dissected on ice in PBS, transferred in 25 μl homogenization buffer (100 mM Na$_2$HPO4–NaH$_2$PO4 at pH 7.2, 2 mM ATP, 2 mM MgCl$_2$), containing 1:100 dilutions of phosphatase- (Sigma) and protease- (Roche Diagnostics, Indianapolis, IN) inhibitor cocktails, and homogenized. Biotinylated phalloidin (Molecular Probes) was added to a final concentration of 0.15 units per brain and incubated with rotation for 30 min at room temperature. Streptavidin-coated magnetic beads (Invitrogen, Carlsbad, CA) were blocked for 30 min in PBS with 5% BSA, washed and resuspended in

homogenization buffer. To isolate biotinylated phalloidin-bound protein complexes, streptavidin-coated beads were added to the extracts and incubated for 30 min at room temperature with rotation. The precipitated material was then washed five times with homogenization buffer, resuspended in SDS loading buffer, analysed by 10% SDS–PAGE and immunoblotted according to standard protocols.

To analyse the total tau levels and the phosphorylation status of tau in different genotypes, adult fly heads at one day post-eclosion were homogenized, separated by SDS–PAGE and analysed by immunoblotting.

The following primary antibodies were used for western blot analysis: rabbit polyclonal anti-actinA-2066 (1:50,000; Sigma), anti-tau (1:100,000; Dako, Carpinteria, CA), monoclonal anti-AT8 (1:10,000; Innogenetics) and anti-PHF-1 (1:10,000; from P. Davies). The appropriate secondary antibody was applied at 1:50,000 dilution and signals were detected by chemiluminescence (Pierce, Rockford, IL).

***In vitro* actin-bundling assay.** Non-muscle actin was purchased from Cytoskeleton, and polymerized into 5–10 μm actin filaments according to manufacturer protocol. Native tau (bovine brain, 90% purity) was also purchased from Cytoskeleton, Inc. Tau actin-bundling activity was determined by a low speed sedimentation assay. F-actin (7 μM) was incubated in the presence or absence of tau protein (~3 μM) for 1 h at room temperature. Samples were then centrifuged at 15,000*g* for 10 min at room temperature to separate actin bundles that pellet (PB) from actin filaments that remain in the supernatant (SN). Equal volumes of supernatants and pellets were analyzed by SDS–PAGE, and protein was detected by Coomassie Blue staining. For the tau immunodepletion experiments, polyclonal anti-tau antibody (Dako) was immobilized on Protein-G magnetic beads (Invitrogen) and tau preparations were incubated with these beads for 2 h at 4 °C. The supernatant was then used as tau sample in the same experimental procedure as above.

F-actin depolymerization assay. For the Swinholide-A–actin depolymerization assay, *in vitro* polymerized F-actin was incubated in the presence or absence of tau for 1 h at room temperature. Samples were then treated with 20 μM final concentration Swinholide-A (Biomol International, Plymouth Meeting, PA) for 1 h at room temperature. Biotinylated phalloidin (0.15 units final concentration) was added to samples and incubated with rotation for 30 min at room temperature. Biotinylated phalloidin-bound protein complexes were then isolated following incubation with streptavidin-coated magnetic beads for 30 min at room temperature with rotation. The supernatant was saved as the G-actin fraction. The precipitated material was washed five times in general actin buffer (Cytoskeleton) and used as the F-actin fraction. Samples were analysed by SDS–PAGE and the actin band was detected by Coomassie Blue staining. Quantification was performed using the ImageJ processing software (NIH, Bethesda, MD).

Transmission and scanning electron microscopy (TEM and SEM). Before centrifugation, small aliquots of the samples from the *in vitro* actin-bundling assays were adsorbed onto Formvar-coated, carbon-stabilized copper grids for 2 min. The grids were negatively stained with 1% uranyl acetate, air-dried and examined with a JEOL 1200 EX transmission electron microscope at an accelerating voltage of 80 kV at a nominal magnification of 49,000.

For SEM, adult flies at one day post-eclosion were dehydrated by overnight incubations in a graded ethanol series. The dehydrated flies were critical point-dried, mounted on SEM stubs, sputter-coated with gold–palladium and examined with a scanning electron microscope.

TUNEL staining. Neuronal apoptosis was determined by nuclear DNA fragmentation as revealed by fluorescent TUNEL staining using a commercially available kit (TdT FragEL; Calbiochem, San Diego, CA). Neurodegeneration was quantified by counting the number of TUNEL positive cells in consecutive 4 μM frontal sections including the entire brain either from 10-day-old flies grown at 21 °C or 20 day-old flies grown at 25 °C. At least four brains were examined for each genotype.

Note: Supplementary Information is available on the Nature Cell Biology website.

ARTICLES

1. Buee, L., Bussiere, T., Buee-Scherrer, V., Delacourte, A. & Hof, P. R. Tau protein isoforms, phosphorylation and role in neurodegenerative disorders. *Brain Res. Brain Res. Rev.* **33,** 95–130 (2000).
2. Lee, V. M., Goedert, M. & Trojanowski, J. Q. Neurodegenerative tauopathies. *Annu. Rev. Neurosci.* **24,** 1121–1159 (2001).
3. Cross, D., Vial, C. & Maccioni, R. B. A tau-like protein interacts with stress fibers and microtubules in human and rodent cultured cell lines. *J. Cell Sci.* **105,** 51–60 (1993).
4. DiTella, M., Feiguin, F., Morfini, G. & Caceres, A. Microfilament-associated growth cone component depends upon Tau for its intracellular localization. *Cell Motil. Cytoskeleton* **29,** 117–130 (1994).
5. Henriquez, J. P., Cross, D., Vial, C. & Maccioni, R. B. Subpopulations of tau interact with microtubules and actin filaments in various cell types. *Cell Biochem. Funct.* **13,** 239–250 (1995).
6. Kempf, M., Clement, A., Faissner, A., Lee, G. & Brandt, R. Tau binds to the distal axon early in development of polarity in a microtubule- and microfilament-dependent manner. *J. Neurosci.* **16,** 5583–5592 (1996).
7. Cunningham, C. C. *et al.* Microtubule-associated protein 2c reorganizes both microtubules and microfilaments into distinct cytological structures in an actin-binding protein-280-deficient melanoma cell line. *J. Cell Biol.* **136,** 845–857 (1997).
8. Zmuda, J. F. & Rivas, R. J. Actin disruption alters the localization of tau in the growth cones of cerebellar granule neurons. *J. Cell Sci.* **113,** 2797–2809 (2000).
9. Griffith, L. M. & Pollard, T. D. The interaction of actin filaments with microtubules and microtubule-associated proteins. *J. Biol. Chem.* **257,** 9143–9151 (1982).
10. Correas, I., Padilla, R. & Avila, J. The tubulin-binding sequence of brain microtubule-associated proteins, tau and MAP-2, is also involved in actin binding. *Biochem J.* **269,** 61–64 (1990).
11. Moraga, D. M., Nunez, P., Garrido, J. & Maccioni, R. B. A tau fragment containing a repetitive sequence induces bundling of actin filaments. *J. Neurochem.* **61,** 979–986 (1993).
12. Farias, G. A., Munoz, J. P., Garrido, J. & Maccioni, R. B. Tubulin, actin, and tau protein interactions and the study of their macromolecular assemblies. *J. Cell Biochem.* **85,** 315–324 (2002).
13. Roger, B., Al-Bassam, J., Dehmelt, L., Milligan, R. A. & Halpain, S. MAP2c, but not tau, binds and bundles F-actin via its microtubule binding domain. *Curr. Biol.* **14,** 363–371 (2004).
14. Schochet, S. S., Jr., Lampert, P. W. & Lindenberg, R. Fine structure of the Pick and Hirano bodies in a case of Pick's disease. *Acta. Neuropathol.* **11,** 330–337 (1968).
15. Goldman, J. E. The association of actin with Hirano bodies. *J. Neuropathol. Exp. Neurol.* **42,** 146–152 (1983).
16. Galloway, P. G., Perry, G. & Gambetti, P. Hirano body filaments contain actin and actin-associated proteins. *J. Neuropathol. Exp. Neurol.* **46,** 185–199 (1987).
17. Hirano, A. Hirano bodies and related neuronal inclusions. *Neuropathol. Appl. Neurobiol.* **20,** 3–11 (1994).
18. Gourlay, C. W., Carpp, L. N., Timpson, P., Winder, S. J. & Ayscough, K. R. A role for the actin cytoskeleton in cell death and aging in yeast. *J. Cell Biol.* **164,** 803–809 (2004).
19. Ohtsu, M. *et al.* Inhibition of apoptosis by the actin-regulatory protein gelsolin. *EMBO J.* **16,** 4650–4656 (1997).
20. Koya, R. C. *et al.* Gelsolin inhibits apoptosis by blocking mitochondrial membrane potential loss and cytochrome *c* release. *J. Biol. Chem.* **275,** 15343–15349 (2000).
21. Chua, B. T. *et al.* Mitochondrial translocation of cofilin is an early step in apoptosis induction. *Nature Cell Biol.* **5,** 1083–1089 (2003).
22. Wittmann, C. W. *et al.* Tauopathy in *Drosophila*: neurodegeneration without neurofibrillary tangles. *Science* **293,** 711–714 (2001).
23. Jackson, G. R. *et al.* Human wild-type tau interacts with wingless pathway components and produces neurofibrillary pathology in *Drosophila*. *Neuron* **34,** 509–519 (2002).
24. Muqit, M. M. & Feany, M. B. Modelling neurodegenerative diseases in *Drosophila*: a fruitful approach? *Nature Rev. Neurosci.* **3,** 237–243 (2002).
25. Nishimura, I., Yang, Y. & Lu, B. PAR-1 kinase plays an initiator role in a temporally ordered phosphorylation process that confers tau toxicity in *Drosophila*. *Cell* **116,** 671–682 (2004).
26. Karsten, S. L. *et al.* A genomic screen for modifiers of tauopathy identifies puromycin-sensitive aminopeptidase as an inhibitor of tau-induced neurodegeneration. *Neuron* **51,** 549–560 (2006).
27. Andorfer, C. *et al.* Hyperphosphorylation and aggregation of tau in mice expressing normal human tau isoforms. *J. Neurochem.* **86,** 582–590 (2003).
28. Andorfer, C. *et al.* Cell-cycle reentry and cell death in transgenic mice expressing nonmutant human tau isoforms. *J. Neurosci.* **25,** 5446–54 54 (2005).
29. Ramsden, M. *et al.* Age-dependent neurofibrillary tangle formation, neuron loss, and memory impairment in a mouse model of human tauopathy (P301L). *J. Neurosci.* **25,** 10637–10647 (2005).
30. Santacruz, K. *et al.* Tau suppression in a neurodegenerative mouse model improves memory function. *Science* **309,** 476–481 (2005).
31. McGough, A., Pope, B., Chiu, W. & Weeds, A. Cofilin changes the twist of F-actin: implications for actin filament dynamics and cellular function. *J. Cell Biol.* **138,** 771–781 (1997).
32. Galloway, P. G., Perry, G., Kosik, K. S. & Gambetti, P. Hirano bodies contain tau protein. *Brain Res.* **403,** 337–340 (1987).
33. Maciver, S. K. & Harrington, C. R. Two actin binding proteins, actin depolymerizing factor and cofilin, are associated with Hirano bodies. *Neuroreport* **6,** 1985–1988 (1995).
34. Spires, T. L. *et al.* Region-specific dissociation of neuronal loss and neurofibrillary pathology in a mouse model of tauopathy. *Am. J. Pathol.* **168,** 1598–1607 (2006).
35. Shulman, J. M. & Feany, M. B. Genetic modifiers of tauopathy in *Drosophila*. *Genetics* **165,** 1233–1242 (2003).
36. Khurana, V. *et al.* TOR-mediated cell-cycle activation causes neurodegeneration in a *Drosophila* tauopathy model. *Curr. Biol.* **16,** 230–241 (2006).
37. Wagner, C. R., Mahowald, A. P. & Miller, K. G. One of the two cytoplasmic actin isoforms in *Drosophila* is essential. *Proc. Natl Acad. Sci. USA* **99,** 8037–8042 (2002).
38. Hardy, J. & Selkoe, D. J. The amyloid hypothesis of Alzheimer's disease: progress and problems on the road to therapeutics. *Science* **297,** 353–356 (2002).
39. Gotz, J., Chen, F., van Dorpe, J. & Nitsch, R. M. Formation of neurofibrillary tangles in P301l tau transgenic mice induced by Aβ 42 fibrils. *Science* **293,** 1491–1495 (2001).
40. Lewis, J. *et al.* Enhanced neurofibrillary degeneration in transgenic mice expressing mutant tau and APP. *Science* **293,** 1487–1491 (2001).
41. Finelli, A., Kelkar, A., Song, H. J., Yang, H. & Konsolaki, M. A model for studying Alzheimer's Aβ42-induced toxicity in *Drosophila melanogaster*. *Mol. Cell. Neurosci.* **26,** 365–375 (2004).
42. Ghosh, S. & Feany, M. B. Comparison of pathways controlling toxicity in the eye and brain in *Drosophila* models of human neurodegenerative diseases. *Hum. Mol. Genet.* **13,** 2011–2018 (2004).
43. Warrick, J. M. *et al.* Expanded polyglutamine protein forms nuclear inclusions and causes neural degeneration in *Drosophila*. *Cell* **93,** 939–949 (1998).
44. Harms, C. *et al.* Neuronal gelsolin prevents apoptosis by enhancing actin depolymerization. *Mol. Cell Neurosci.* **25,** 69–82 (2004).
45. Zhu, X. *et al.* Oxidative stress signalling in Alzheimer's disease. *Brain Res.* **1000,** 32–39 (2004).
46. Rodriguez, O. C. *et al.* Conserved microtubule-actin interactions in cell movement and morphogenesis. *Nature Cell Biol.* **5,** 599–609 (2003).
47. Niwa, R., Nagata-Ohashi, K., Takeichi, M., Mizuno, K. & Uemura, T. Control of actin reorganization by Slingshot, a family of phosphatases that dephosphorylate Alzheimer's diseaseF/cofilin. *Cell* **108,** 233–246 (2002).
48. Lee, T. & Luo, L. Mosaic analysis with a repressible cell marker for studies of gene function in neuronal morphogenesis. *Neuron* **22,** 451–461 (1999).
49. Dias-Santagata, D., Fulga, T. A., Duttaroy, A. & Feany, M. B. Oxidative stress mediates tau-induced neurodegeneration in *Drosophila*. *J. Clin. Invest.* **117,** 236–245 (2007).
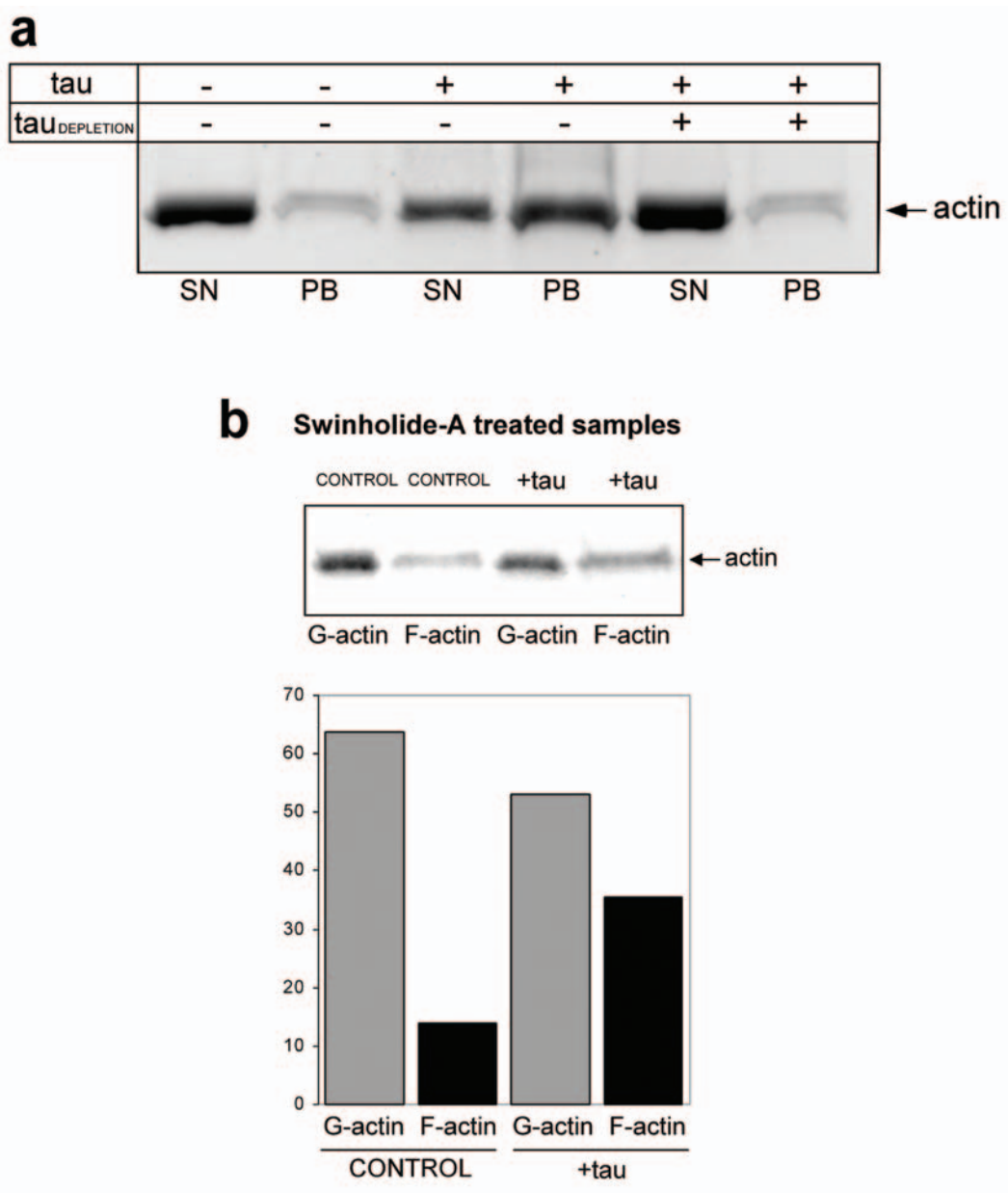
Figure S1 (**a**) Incubation of actin filaments with tau results in formation of bundled actin filaments detected in the pellet fraction (PB) while individual filaments remain in the supernatant (SN). In samples from which tau has been removed by immunodepletion no bundling effect was observed. Samples were separated on SDS-PAGE and detected by Coomassie Blue staining. (**b**) Incubation of *in vitro* polymerized actin filaments with tau results in increased resistance to treatment with the actin depolymerization drug Swinholide A. Samples were detected by Commassie blue staining and the intensity of the actin bands was quantified using the ImageJ analysis software. Tau treated samples show higher levels of filamentous actin compared to control, non-treated, samples.
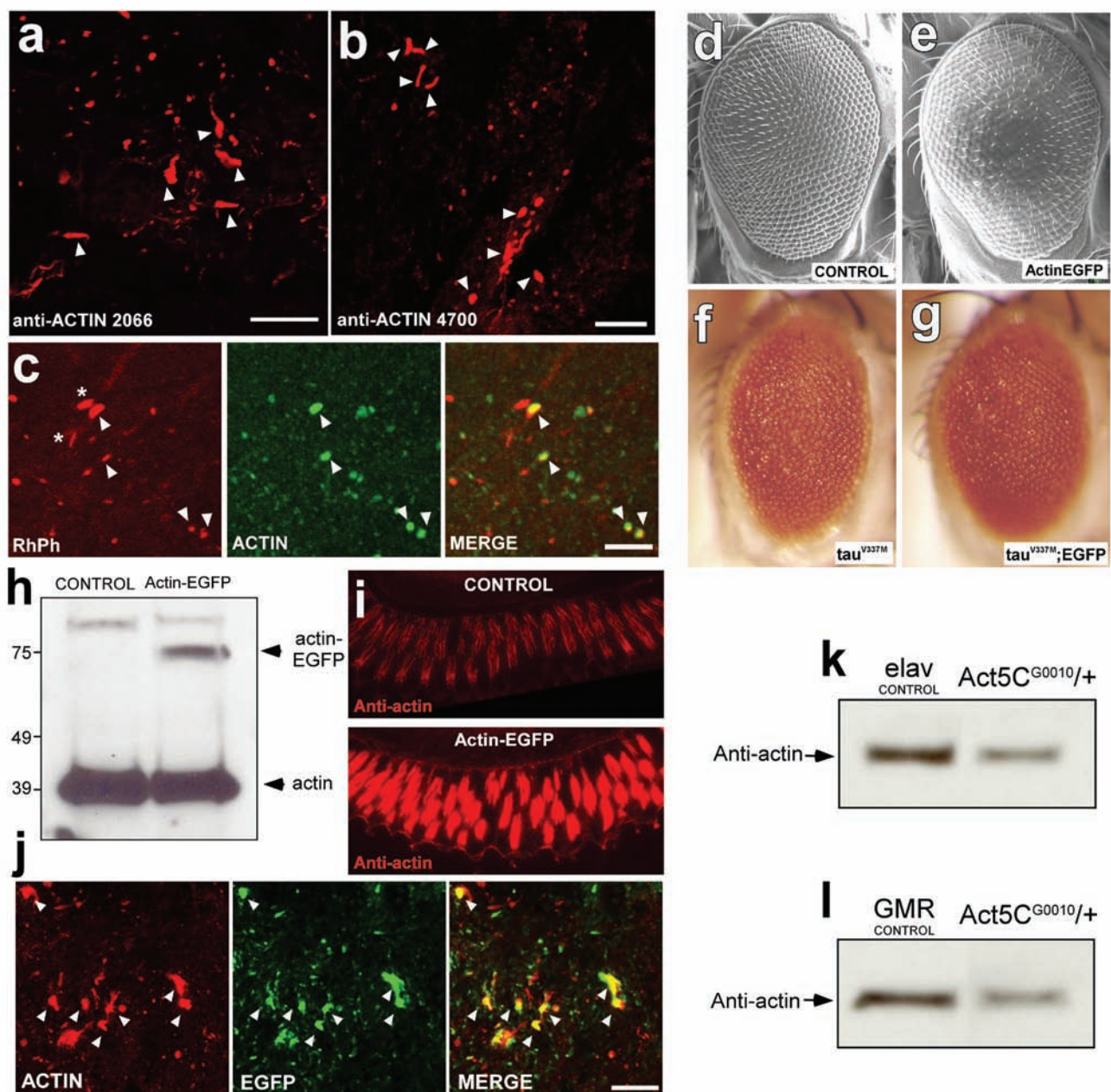
Figure S2 (**a** – **b**) Immunofluorescence of frontal brain sections from tau transgenic flies stained with either an anti-actin polyclonal rabbit antibody (Sigma A-2066) (**a**) or an anti-actin mouse monoclonal antibody (Sigma A-4700) (**b**). Actin-rich rod-like structures are revealed by both antibodies. (**c**) Tau transgenic whole mount brains double stained with rhodamine phalloidin and actin antibody A-2066. The majority of the actin antibody-positive structures are highlighted by RhPh (arrowheads). A small percentage of rods stain with RhPh but not with the actin antibody (*). (**d** – **e**) SEM of a control (*GMR-GAL4/+*) (**d**) and an actin transgenic fly eye (*GMR-GAL4/UAS-Act5C-EGFP*) (**e**). (**f** – **g**) Retinal toxicity in flies expressing tau^{V337M} (**f**) or co-expressing tau^{V337M} and *UAS-EGFP* (**g**) under the control of the *GMR-GAL4* driver. No change in retinal toxicity is observed in the double transgenic flies compared to single transgenic tau flies. (**h**) Total actin levels from head extracts from control flies (*GMR-GAL4/+*) or flies overexpressing actin-EGFP under the *GMR-GAL4* driver (*GMR-GAL4/UAS-Act5C-EGFP*). The image represents a western blot probed with an anti-actin antibody. Ectopically expressed actin-EGFP fusion protein migrates at a higher molecular weight. (**i**) Immunofluorescence analysis using anti-actin antibody A-2066 of retinal neurons in paraffin-embedded tissue sections of the same genotypes as in (**h**). (**j**) Actin rods in frontal brain sections from flies co-expressing tau^{R406W} with actin-EGFP, and double labeled for actin (red) and EGFP (green). Scale bars are 10 μm. (**k** – **l**) Total actin levels from head extracts from control flies (*GMR-GAL4/+*) (**k**) or (*elav-GAL4/+*) (**l**) and flies heterozygous for an actin null allele (*Act5C^{G0010}*). The images represent western blots probed with anti-actin antibody A-2066. Scale bars are 10 μm in **a** and **b** and 5 μm in **c** and **j**.
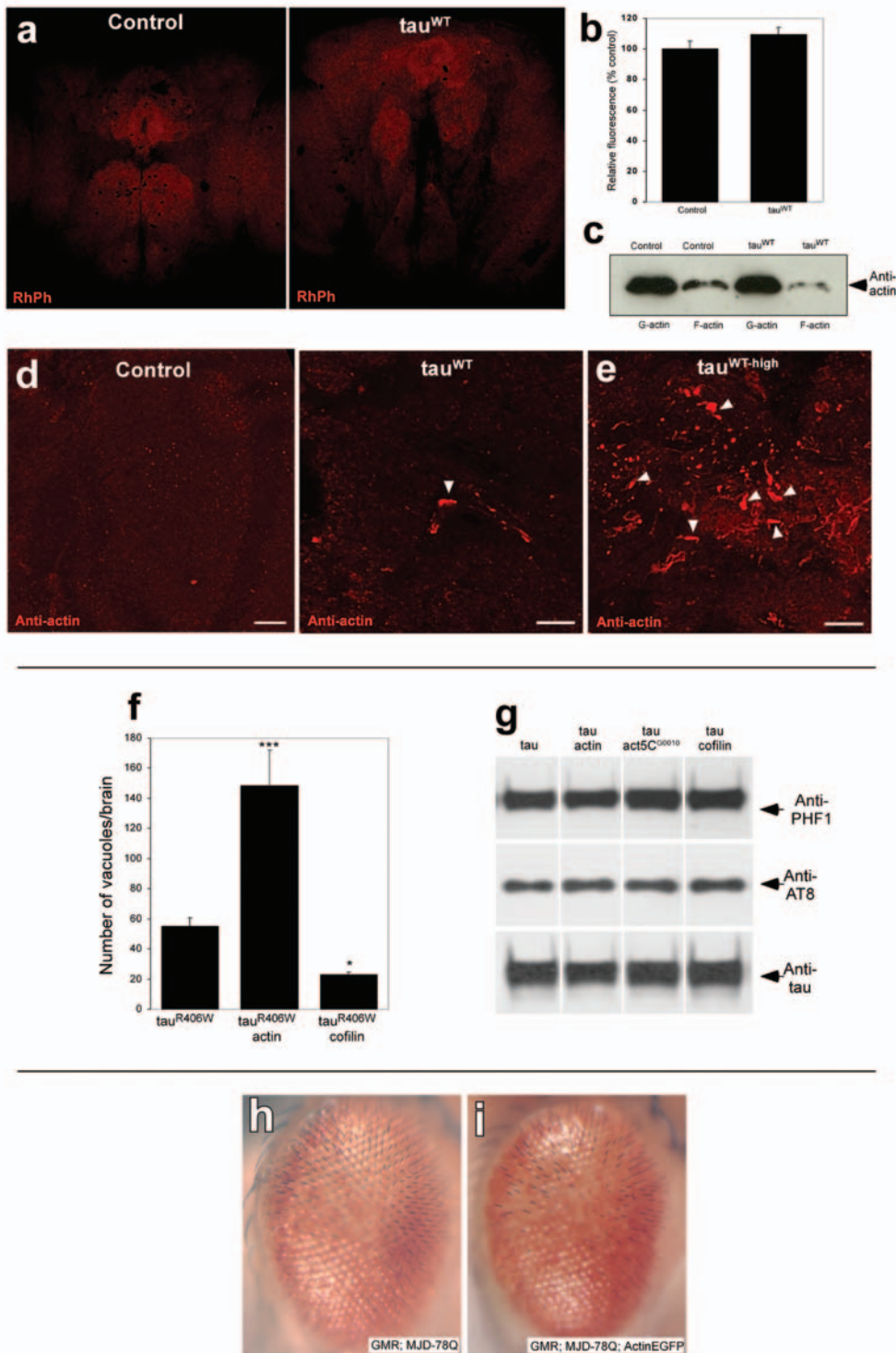
Figure S3 (**a**) F-actin staining of whole mount brains from control flies compared to tau^{WT} transgenic flies (tau^{WT}). (**b**) Quantitative analysis of fluorescence intensities averaged from three distinct areas of the brain using the MetaMorph software (unpaired t-test; p=0.2). Error bars are +/- SEM. (**c**) Total G-actin and F-actin levels isolated from fresh brain extracts of control and tau^{WT} flies. Images represent Western blots using an antibody to actin. (**d** – **e**) Immunofluorescence using an actin antibody of frontal brain sections from control non-transgenic flies or tau^{WT} transgenic flies expressing moderate and high levels of tau protein. Only occasional rods are formed in flies expressing moderate levels of tau (**d**) but they are abundant in flies expressing tau at high levels (**e**) (arrowheads). Scale bars are 10 μm. (**f**)

Quantification of number of vacuoles as revealed by hematoxylin and eosin staining in tau^{R406W} transgenic flies compared to flies coexpressing tau^{R406W} with actin and flies coexpressing tau^{R406W} with cofilin (one-way ANOVA with Student-Neuman-Keuls; ***p<0.001; *p<0.05). Error bars are +/- SEM. (**f**) Western blot analysis of head extracts from transgenic flies expressing tau, tau and an actin transgene, tau in a genetic background heterozygous for a null actin allele, or tau and a cofilin transgene, using two phosphorylation-dependent tau antibodies (anti-AT8 and anti-PHF1). Blots were stripped and re-probed for total tau protein (anti-TAU). (**h** – **i**) Comparable eye degeneration and depigmentation in MJD-78Q transgenic flies (**h**) and flies co-expressing MJD-78Q with an actin transgene (**i**).
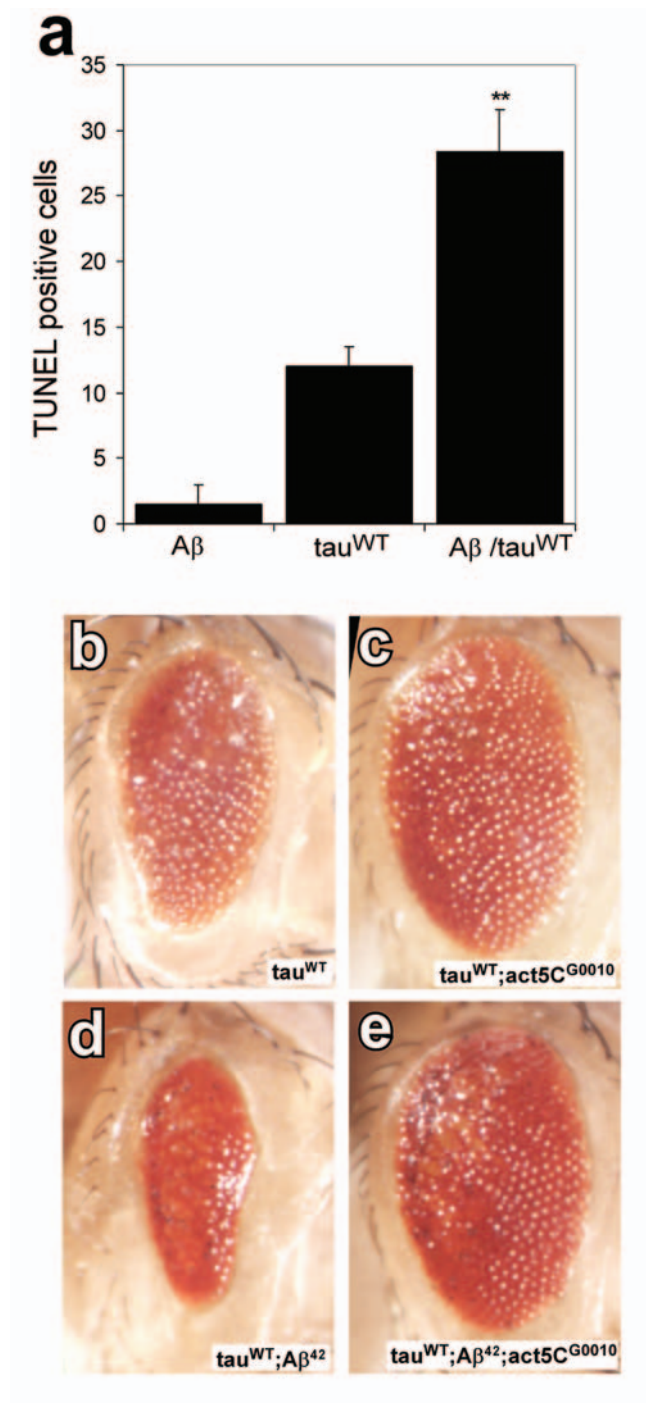
Figure S4 Quantification of TUNEL-positive neurons in brain of flies panneurally expressing tau^{WT}, Aβ or co-expressing tau^{WT} and Aβ (one-way ANOVA with Student-Neuman-Keuls; **p<0.01). Error bars are +/- SEM. All flies were aged to 10 days. **b-e**, Retinal toxicity in flies expressing tau^{WT} alone (**a**), tau^{WT} in a genetic background heterozygous for *Act5C^{G0010}* null actin allele (**b**), double transgenic flies expressing tau^{WT} and Aβ (**c**), and flies co-expressing tau and Aβ in a background heterozygous for *Act5C^{G0010}* actin allele (**d**).